Limiting performance analysis of cascaded interband/intersubband thermophotovoltaic devices

Jian Yin and Roberto Paiella[a)]

Department of Electrical and Computer Engineering and Photonics Center, Boston University, 8 Saint Mary's Street, Boston, Massachusetts 02215, USA

(Received 15 October 2010; accepted 6 January 2011; published online 24 January 2011)

This work addresses the question of how much electrical power can in principle be extracted from heat radiation via the combined use of interband and intersubband photodetection as a way to overcome the fundamental limitations of existing thermophotovoltaic devices using mature InP-based technology. Very efficient coverage of the incident radiation spectrum and optimal current matching can be achieved using multiple quantum-cascade structures monolithically integrated with a *p-n* junction by taking advantage of their intrinsic cascading scheme, spectral agility, and design flexibility. Numerical simulations indicate that this approach can effectively double the present state-of-the-art in thermophotovoltaic output electrical power. © *2011 American Institute of Physics*. [doi:10.1063/1.3548672]

Thermophotovoltaic (TPV) energy conversion is a promising approach for waste heat harvesting and clean energy production in a wide range of environments.[1–4] Its basic idea is to use infrared photovoltaic devices to extract electrical power from heat radiation originating from thermal sources at typical temperatures of 1000–1500 °C. Existing TPV systems normally employ InGaAs(Sb) or GaSb single-junction photodiodes, whose bandgap energy E_g is sufficiently small to enable absorption of a large fraction of the incident thermal photons. In particular, the current laboratory state-of-the-art is based on InGaAs photodiodes with $E_g \approx 0.6$ eV, grown lattice mismatched on InP with an InPAs buffer.[1]

Similar to the case of solar cells, the conversion efficiency of single-junction TPV devices is ultimately determined by two limiting factors. First, below-bandgap photons cannot be absorbed and therefore their energy cannot be harvested. Second, while high-energy photons are efficiently absorbed, only a fraction of their energy is converted into electricity, with the remainder lost to the lattice as the resulting photocarriers relax to the bottom of their respective bands before being collected. These limitations can be overcome with the use of cascaded multiple junctions of different bandgap energy, each providing efficient conversion of near-bandgap radiation over a different wavelength range. However, semiconductors of widely different bandgap energies typically also feature proportionally different lattice constants, so that the number of different *p-n* junctions that can be grown on top of one another is limited in practice by strain accumulation. In fact, tandem TPV devices have so far failed to improve on the performance of optimized single-junction photodiodes.[2]

An alternative approach to the development of infrared photovoltaic devices is the use of intersubband (ISB) transitions in suitably designed quantum-cascade (QC) structures. Photodetectors based on this approach have already been demonstrated with a variety of quantum-well (QW) materials systems for thermal imaging applications,[5–7] and typically involve a cascade of several identical repeat units (stages). At the same time, some of the basic properties of QC structures are also ideally suited to the development of high-efficiency "multiple-junction" TPV devices. In particular, their operation wavelength can be tuned by design over a broad range using the same QW materials system, so that an arbitrary number of different stages absorbing at different wavelengths can be grown on top of one another without strain accumulation.[7] Furthermore, each stage provides absorption over a relatively narrow spectral region, so that the energy of all absorbed photons can be extracted with high efficiency. The resulting potential of QC structures for TPV energy conversion has been highlighted and numerically investigated in a recent study.[8] A similar idea based on interband cascade structures has also been recently investigated.[9]

In this work we address the question of how much electrical power can in principle be extracted from a typical TPV heat-radiation source by combining interband and ISB photovoltaic energy conversion within the same device. To that purpose, we consider an $In_{0.67}Ga_{0.33}As$ *p-n* junction (i.e., with $E_g \approx 0.6$ eV as in Ref. 1) monolithically integrated with different QC stages based on large-conduction-band-offset $In_{0.83}Ga_{0.17}As/AlAs_{0.65}Sb_{0.35}$ QWs. With this choice of compositions the average equilibrium lattice constant of the QC active material is approximately the same as that of the *p-n* junction, so that no net strain accumulates across the device and the resulting performance degradation due to defect formation can be avoided.[10] The *p-n* junction allows harvesting the high-energy incident thermal photons that cannot be absorbed in the QC active material due to the finite conduction-band offset ΔE_c of the QWs.[11] At the same time, the individual QC stages are designed to be current-matched to one another and to the underlying interband absorber so as to maximize their combined output electrical power.

A schematic band diagram of this TPV material is shown in Fig. 1, together with the cross-sectional view of a suitable device geometry. The $In_{0.67}Ga_{0.33}As$ *p-n* junction is grown *p*-side down on a semi-insulating InPAs-buffer/InP-substrate combination,[1] followed by the QC active material. The input thermal radiation is coupled in at normal incidence through the optically transparent substrate, so that the high-energy photons can be immediately absorbed in the *p-n* junction. The resulting photoelectrons are swept by the junction

[a)]Electronic mail: rpaiella@bu.edu.

 © 2011 American Institute of Physics

Author complimentary copy. Redistribution subject to AIP license or copyright, see http://apl.aip.org/apl/copyright.jsp

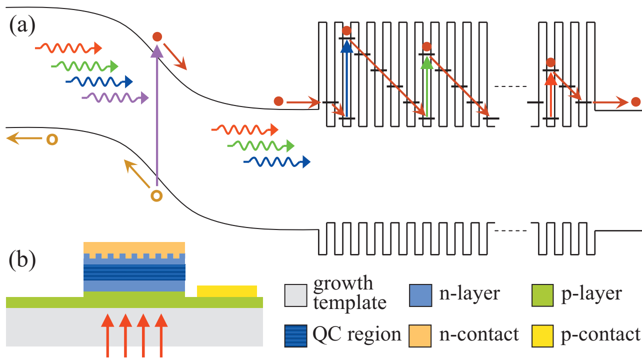

FIG. 1. (Color) (a) Schematic band diagram of a cascaded interband/ISB TPV active material under short-circuit conditions. (b) Cross-sectional view of a possible device geometry based on this material.

built-in electric field toward the ISB absorption region where they are injected into the QC stages, while the photoholes are collected through the *p*-side contact without having to traverse the QWs. Due to the polarization selection rules of ISB transitions (which can only couple to TM-polarized light), the remaining lower-energy photons cannot be directly absorbed in the QC active material as they propagate along the growth axis. Thus, a two-dimensional reflection grating fabricated on the device top surface is used to scatter these photons into the TM guided modes supported by the epitaxial layer on InP. ISB photodetectors with near-unity quantum efficiency under unpolarized normal-incidence illumination can be realized with this approach, as demonstrated in previous work.[12]

The device modeled in this study comprises four different QC structures, labeled QC1–QC4, whose individual-layer thicknesses are listed in Table I. In Fig. 2 we plot the Γ-point conduction-band lineup of two repetitions of structure QC2 in the presence of photovoltage, together with the squared envelope functions of the relevant bound states (referenced to their respective energy levels). In this structure photoelectrons are created via ISB transitions from the lowest two bound states of a pair of coupled QWs (states $|1\rangle$ and $|2\rangle$ in the figure) to the "continuum" of a chirped superlattice miniband (indicated by the shaded areas). After rapidly relaxing to the bottom of the miniband, the electrons are transported into the next stage via LO-phonon-assisted transitions through the intervening staircase of bound states. The key advantage of this bound-to-continuum design is that it allows

TABLE I. Layer thicknesses of the QC structures designed in this work in units of Å, starting from the coupled-QW absorption region and moving in the direction of the photocurrent. The bold numbers correspond to the barriers and the underlined numbers indicate the *n*-doped layers, with the doping density specified in multiples of 10^{18} cm^{-3} by the subsequent number in parentheses.

	Thickness (Å) [Doping density (10^{18} cm^{-3})]
QC1	**14** 36.5(2) **12** 36.5 **15** 30 **15** 26 **15** 23 **15** 20.5 **16** 18 **16** 16 **16** 15 **15** 13 **14** 12 **15** 12 **15** 12
QC2	**17** 45(1.3) **14** 44 **19** 37 **14** 32 **14** 28.5 **15** 25 **15** 22.5 **15** 20 **15** 19 **16** 15.5 **15.5** 15.5 **15.5** 15.5
QC3	**16** 53(0.8) **14** 52 **16** 43 **12** 36 **12** 31 **13** 27 **13** 24.5 **13** 21 **12** 19.5 **14** 19.5 **14** 19.5
QC4	**14.5** 64(0.7) **12** 63 **15** 50 **11** 42 **12** 37 **13** 33 **14** 28.5 **12** 24.5 **13.5** 24.5 **13.5** 24.5

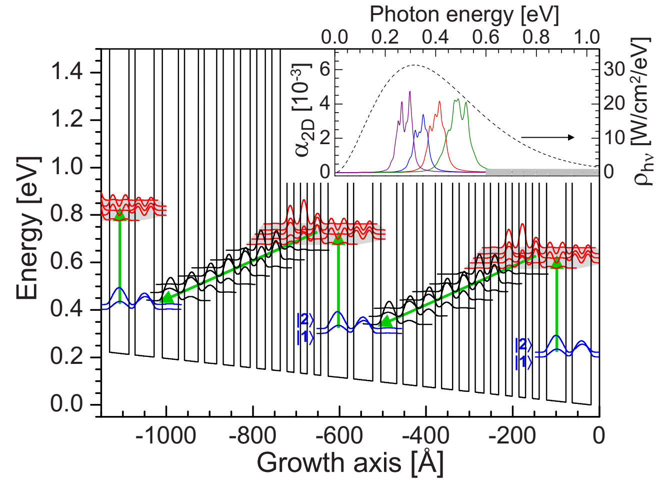

FIG. 2. (Color online) Γ-valley conduction-band lineup of two adjacent stages based on the QC2 design in Table I and squared envelope functions of the relevant bound states. The processes of photon absorption and photocarrier collection are illustrated by the vertical and diagonal arrows, respectively. Inset: normalized ISB absorption spectra α_{2D} of the four QC structures in Table I. The dashed curve is the radiated intensity spectrum $\rho_{h\nu}$ (per unit photon energy) of a blackbody source at 1300 K. The gray line near the horizontal axis indicates the absorption band of the $In_{0.67}Ga_{0.33}As$ *p*-*n* junction.

tuning the absorption linewidth, and hence the amount of photocurrent produced by each stage, for the purpose of current matching.

To evaluate the electrical characteristics of the device under study, the room-temperature photocurrent and dark-current densities J_p and J_d produced by each "junction" (both interband and ISB) were calculated as a function of voltage V across the same junction. All material parameters used in these simulations were taken from Refs. 13 and 14, and incident radiation from a blackbody source at a representative temperature of 1300 K was assumed. J_p was computed for the ideal case where every incident photon with energy within the junction absorption band is absorbed (as is commonly assumed for the purpose of evaluating the limiting performance of photovoltaic devices). In the case of the *p*-*n* junction, the absorption band was taken to be the spectral range $h\nu > E_g$. In the case of each QC stage, its ISB absorption spectrum $\alpha_{2D}(h\nu)$ was first calculated, and the absorption band was then taken as the spectral range where α_{2D} (normalized to the stage inverse thickness) is larger than 2×10^{-3}. As discussed in Ref. 8, this threshold value is sufficiently large to justify the assumption of complete absorption within the envisioned device geometry. The calculated absorption spectra of the four QC structures in Table I are plotted in the inset of Fig. 2. By design, when combined with the $In_{0.67}Ga_{0.33}As$ *p*-*n* junction these structures cover a very large fraction of the incident 1300–K blackbody radiation spectrum $\rho_{h\nu}$, which is also shown in the figure.

The dark-current density of the *p*-*n* junction was computed using the ideal diode equation with a reverse saturation current density of 0.4 $\mu A/cm^2$, as measured in the 0.6–eV bandgap-energy InGaAs photodiode of Ref. 1. In the case of the QC stages, $J_d(V)$ was evaluated using the theoretical model developed in Ref. 6, based on the net transfer of electrons between consecutive stages via LO-phonon scattering. The key assumption behind this model is the presence of quasi-thermal equilibrium within each "cascade" of highly

Author complimentary copy. Redistribution subject to AIP license or copyright, see http://apl.aip.org/apl/copyright.jsp

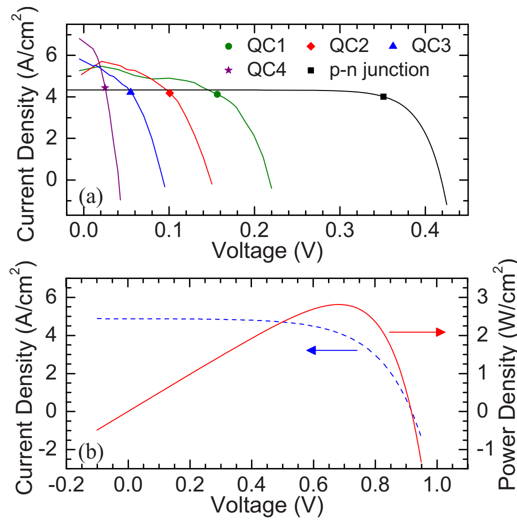

FIG. 3. (Color online) (a) Total current density $J_{tot} \equiv J_p - J_d$ vs voltage V for the *p-n* junction and for the four QC structures in Table I in the presence of 1300–K blackbody radiation. (b) Total current density $J_{tot} \equiv J_p - J_d$ vs combined voltage V_{tot} for the cascaded interband/ISB device comprising the individual junctions of (a) (dashed line) and corresponding output power density $P = J_{tot} V_{tot}$ vs V_{tot} (solid line).

connected states in each stage, which is justified by the particularly fast ISB relaxation among these states.

The resulting electrical characteristics ($J_{tot} \equiv J_p - J_d$ versus V) of the *p-n* junction and of the four QC stages are plotted in Fig. 3(a). The symbol on each trace indicates the operating point where the electrical power density produced individually by the corresponding junction (given by the product $J_{tot}V$) is maximum. By design, these operating points all occur at roughly the same current density of about 4 A/cm^2, i.e., the individual junctions of the interband/ISB TPV device under study are optimally current-matched to one another. The electrical characteristics of this multiple-junction device were finally obtained by adding the voltages V of the individual junctions for each value of J_{tot}, starting from exponential fits to the traces of Fig. 3(a). The result is shown in Fig. 3(b) (dashed line), together with the corresponding output power density $P = J_{tot} V_{tot}$ plotted versus total voltage V_{tot} (solid line). The short-circuit current density, open-circuit voltage, and fill factor obtained from these traces are 4.9 A/cm^2, 0.92 V, and 63%, respectively; the maximum output electrical power density is over 2.8 W/cm^2.

By comparison, the present state-of-the-art in TPV energy conversion from a thermal source at the same temperature of 1300 K is about 0.8 W/cm^2, obtained with a photodiode based on the same InGaAs *p-n* junction studied in this work.[1] According to our simulation results in Fig. 3(a), the output power density $J_{tot}V$ of such a *p-n* junction when used by itself is limited to a maximum theoretical value of about 1.4 W/cm^2. We therefore conclude that the monolithic integration of interband and ISB photovoltaic junctions has the potential to effectively double the present state-of-the-art in TPV output power. At the same time, it can be used to optimize the tradeoff between output power and conversion efficiency, which depends on the specific TPV system configuration such as the use of spectral control to recuperate the unabsorbed radiation. The results presented in this study should therefore strongly motivate the experimental development of such a novel family of TPV devices.

This work was partly supported by the NSF under Grant No. ECCS-0824116.

[1] B. Wernsman, R. R. Siergiej, S. D. Link, R. G. Mahorter, M. N. Palmisiano, R. J. Wehrer, R. W. Schultz, G. P. Schmuck, R. L. Messham, S. Murray, C. S. Murray, F. Newman, D. Taylor, D. M. DePoy, and T. Rahmlow, IEEE Trans. Electron Devices **51**, 512 (2004).
[2] R. R. Siergiej, S. Sinharoy, T. Valko, R. J. Wehrer, B. Wernsman, S. D. Link, R. W. Schultz, and R. L. Messham, AIP Conf. Proc. **738**, 480 (2004).
[3] M. W. Dashiell, J. F. Beausang, H. Ehsani, G. J. Nichols, D. M. DePoy, L. R. Danielson, P. Talamo, K. D. Rahner, E. J. Brown, S. R. Burger, P. M. Fourspring, W. F. Topper, Jr., P. F. Baldasaro, C. A. Wang, R. K. Huang, M. K. Connors, G. W. Turner, Z. A. Shellenbarger, G. Taylor, J. Li, R. Martinelli, D. Donetski, S. Anikeev, G. L. Belenki, and S. Luryi, IEEE Trans. Electron Devices **53**, 2879 (2006).
[4] L. Bhusal and A. Freundlich, J. Appl. Phys. **102**, 074907 (2007).
[5] M. Graf, G. Scalari, D. Hofstetter, J. Faist, H. Beere, E. Linfield, D. Ritchie, and G. Davies, Appl. Phys. Lett. **84**, 475 (2004).
[6] C. Koeniguer, G. Dubois, A. Gomez, and V. Berger, Phys. Rev. B **74**, 235325 (2006).
[7] D. Hofstetter, F. R. Giorgetta, E. Baumann, Q. Yang, C. Manz, and K. Köhler, Appl. Phys. Lett. **93**, 221106 (2008).
[8] J. Yin and R. Paiella, Opt. Express **18**, 1618 (2010).
[9] R. Q. Yang, Z. Tian, J. F. Klem, T. D. Mishima, M. B. Santos, and M. B. Johnson, Appl. Phys. Lett. **96**, 063504 (2010).
[10] The individual well and barrier layers here are under compressive and tensile strain, respectively, by less than 1.7%. This is smaller than the individual-layer strain of the $In_{0.7}Ga_{0.3}As/AlAs_{0.8}Sb_{0.2}$ QWs strain-compensated on InP that have already been used to demonstrate high-performance QC lasers, in, e.g., S. Y. Zhang, D. G. Revin, J. W. Cockburn, K. Kennedy, A. B. Krysa, and M. Hopkinson, Appl. Phys. Lett. **94**, 031106 (2009).
[11] In this materials system ΔE_c is estimated to be about 0.80 eV, as determined by the difference between the X-valley minima in the $AlAs_{0.65}Sb_{0.35}$ barriers and the Γ-valley minimum in the $In_{0.83}Ga_{0.17}As$ wells. At the same time, the threshold for interband absorption in all the QC structures designed in this work is larger than the bandgap energy of 0.6 eV of the underlying $In_{0.67}Ga_{0.33}As$ *p-n* junction.
[12] J. Y. Andersson and L. Lundqvist, Appl. Phys. Lett. **59**, 857 (1991).
[13] I. Vurgaftman, J. R. Meyer, and L. R. Ram-Mohan, J. Appl. Phys. **89**, 5815 (2001).
[14] *Semiconductors—Basic Data*, edited by O. Madelung (Springer, Berlin, 1996).

Author complimentary copy. Redistribution subject to AIP license or copyright, see http://apl.aip.org/apl/copyright.jsp